PNAS RESEARCH ARTICLE | PHARMACOLOGY

Small-molecule IKKβ activation modulator (IKAM) targets MAP3K1 and inhibits pancreatic tumor growth

John Victor Napoleon[a], Satish Sagar[a], Sydney P. Kubica[a], Lidia Boghean[a], Smit Kour[a], Hannah M. King[a], Yogesh A. Sonawane[a], Ayrianne J. Crawford[a], Nagsen Gautam[b], Smitha Kizhake[a], Pawel A. Bialk[c], Eric Kmiec[c], Jayapal Reddy Mallareddy[a], Prathamesh P. Patil[a], Sandeep Rana[a], Sarbjit Singh[a], Janani Prahlad[a], Paul M. Grandgenett[a], Gloria E. O. Borgstahl[a], Gargi Ghosal[d], Yazen Alnouti[b], Michael A. Hollingsworth[a,e], Prakash Radhakrishnan[a,e], and Amarnath Natarajan[a,b,d,e,1]

Edited by Natalie Ahn, University of Colorado, Boulder, CO; received August 15, 2021; accepted March 29, 2022

Activation of inhibitor of nuclear factor NF-κB kinase subunit-β (IKKβ), characterized by phosphorylation of activation loop serine residues 177 and 181, has been implicated in the early onset of cancer. On the other hand, tissue-specific IKKβ knockout in Kras mutation-driven mouse models stalled the disease in the precancerous stage. In this study, we used cell line models, tumor growth studies, and patient samples to assess the role of IKKβ and its activation in cancer. We also conducted a hit-to-lead optimization study that led to the identification of 39-100 as a selective mitogen-activated protein kinase kinase kinase (MAP3K) 1 inhibitor. We show that IKKβ is not required for growth of Kras mutant pancreatic cancer (PC) cells but is critical for PC tumor growth in mice. We also observed elevated basal levels of activated IKKβ in PC cell lines, PC patient-derived tumors, and liver metastases, implicating it in disease onset and progression. Optimization of an ATP noncompetitive IKKβ inhibitor resulted in the identification of 39-100, an orally bioavailable inhibitor with improved potency and pharmacokinetic properties. The compound 39-100 did not inhibit IKKβ but inhibited the IKKβ kinase MAP3K1 with low-micromolar potency. MAP3K1-mediated IKKβ phosphorylation was inhibited by 39-100, thus we termed it IKKβ activation modulator (IKAM) 1. In PC models, IKAM-1 reduced activated IKKβ levels, inhibited tumor growth, and reduced metastasis. Our findings suggests that MAP3K1-mediated IKKβ activation contributes to KRAS mutation-associated PC growth and IKAM-1 is a viable pretherapeutic lead that targets this pathway.

MAP3K1 | quinoxaline | IKKβ | NF-κB | pancreatic cancer

Significance

Pancreatic cancer is a deadly disease with limited therapeutic options. High expression of the kinase MAP3K1 is associated with poor survival among pancreatic cancer patients. MAP3K1 activates the kinase IKKβ, and our studies show that higher levels of activated IKKβ are found in patient-derived tumors as opposed to the surrounding normal tissue. We also show that inhibition of MAP3K1 by a drug-like compound 39-100 results in reduced levels of activated IKKβ. This leads to reduced tumor growth and reduced metastasis in pancreatic cancer models. Therefore, drug candidates like 39-100, that are IKKβ activation modulators, can be developed to treat pancreatic cancer.

The IKK complex is composed of three subunits, namely IKKα, IKKβ, and IKKγ. The IKK complex serves as the signaling node to regulate NF-κB–mediated gene expression, in response to upstream signals. The canonical NF-κB pathway is regulated by the activation of IKKβ. The hallmark of IKKβ activation is the phosphorylation of its activation loop serine residues 177 and 181 (1). Immunohistochemistry (IHC) studies and genetic mouse models implicate activated IKKβ as a driver of oncogenesis. For example, elevated levels of p-IKKβ were observed in ∼50% of surgically resected tumor samples and tissue-specific expression of constitutively active (ca) IKKβ (S177E, S181E), either in the presence of a mutant oncogene (KrasG12D) or loss of tumor suppressor (APC), resulted in severely compromised survival of mice (2–4). Moreover, tissue-specific inactivation of IKKβ in Kras mutation-driven mouse tumor models resulted in improved survival (5–8). Although the exact mechanism of IKKβ activation is yet to be fully elucidated, upstream kinases, such as MAP3K1 (MEKK1), priming phosphorylation by TAK1 followed by autophosphorylation and oligomerization of regulatory subunit IKKγ (NEMO)-induced transautophosphorylation, have been reported as mechanisms that result in IKKβ activation (9–11).

The link between IKKβ and chronic inflammation led the pharmaceutical industry to vigorously pursue the development of small-molecule IKKβ inhibitors. Nearly all the IKKβ inhibitors developed were ATP competitive and block stimulus induced activation of IKKβ. Despite full characterization of these ATP-competitive IKKβ inhibitors in preclinical models, only four inhibitors entered clinical trials and the Food and Drug Administration has approved none of them, due among others to unfavorable safety profile, lack of efficacy, or portfolio repositioning (7, 12–16). Other strategies explored include NEMO binding peptide to disrupt the IKK complex, resulting in the inhibition of IKKβ activation and a TAK1 inhibitor to block tumor necrosis factor-α (TNF-α)–induced IKKβ activation (17, 18).

The IKBKB gene codes for 756 amino acids (aa), with 16 to 309 aa adopting a classic kinase domain, 310 to 404 aa adopting a ubiquitin fold labeled as ubiquitin-like

Author contributions: E.K., Y.A., and A.N. designed research; J.V.N., S. Sagar, S.P.K., L.B., S. Kour, H.M.K., Y.A.S., A.J.C., N.G., S. Kizhake, P.A.B., J.R.M., P.P., S.R., S. Singh, J.P., and G.G. performed research; J.V.N., J.P., P.M.G., G.E.O.B., and M.A.H. contributed new reagents/analytic tools; J.V.N., S. Sagar, S.P.K., L.B., S. Kour, H.M.K., Y.A.S., A.J.C., N.G., S. Kizhake, P.A.B., E.K., J.R.M., P.P., S.R., S. Singh, G.E.O.B., G.G., Y.A., P.R., and A.N. analyzed data; and J.V.N., S. Kizhake, G.G., P.R., and A.N. wrote the paper.

Competing interest statement: A.N. is named as an inventor on pending US Patent Application No. 16/766,762 filed by the Board of Regents of the University of Nebraska related to this work.

This article is a PNAS Direct Submission.

[1]To whom correspondence may be addressed. Email: anatarajan@unmc.edu.

This article contains supporting information online at http://www.pnas.org/lookup/suppl/doi:10.1073/pnas.2115071119/-/DCSupplemental.

Published April 27, 2022.

domain, and 410 to 664 aa forming the scaffold dimerization domain (SDD) that adopts a helical blade structure. To date, only three groups have reported the structure of IKKβ that extends to the SDD (19–21). The human IKKβ (PDB ID code 4KIK) structure (1-664) is a dimer in which the activation loop (S^{177} and S^{181}) is phosphorylated in protomer B (active form) but not in protomer A (21). The kinase domains of the two protomers are identical and inhibitors that target the ATP binding site are not likely to distinguish between inactive and active IKKβ. However, the protomer conformations are different outside the kinase fold, such as the ∼120 $Å^2$ pocket at the interface of the kinase domain–SDD is open in protomer B (active IKKβ) but is partially closed in protomer A (resting IKKβ), thus providing allosteric sites for inhibitor design (21).

We previously reported a quinoxaline urea analog (13-197) as an allosteric IKKβ inhibitor that inhibited tumor growth and metastasis in an orthotopic pancreatic tumor model and increased median survival of mice in a mantle cell lymphoma (MCL) model (22–24). Here we assessed the role of IKKβ and its activation in a pancreatic cancer (PC) setting and optimized 13-197 to address stability and bioavailability issues for therapy. Toward the former, we show that: 1) IKKβ is dispensable for growth in a PC cell line model but is required for PC tumor growth; 2) the activation–deactivation of IKKβ is transient in normal cells, however the activation is sustained in PC cells; and 3) elevated levels of p-IKKβ are observed in patient-derived pancreatic tumors and liver metastases when compared to adjacent normal tissue. Toward the latter, we show that: 1) hit-to-lead optimization of 13-197 led to novel chemical entity (NCE) 39-100 with improved stability and oral bioavailability; 2) mechanism of action studies revealed that 39-100 is a selective MAP3K1 inhibitor that blocked IKKβ activation, which we termed IKKβ activation modulator 1 (IKAM-1); and 3) oral dosing of IKAM-1 reduced levels of p-IKKβ in tumors, and inhibits tumor growth and metastasis in orthotopic PC models. Our findings suggest that MAP3K1-mediated IKKβ activation contributes to KRAS mutation-associated PC growth and IKAM-1 is a viable pretherapeutic lead that targets this pathway.

Results

The major goal of this study was twofold: 1) to explore the role of activated IKKβ in cellular and animal models and 2) to develop a suitable pretherapeutic lead that inhibits tumor growth by modulating the levels of activated IKKβ.

Role of IKKβ in PC. Despite numerous mouse models that explored the role of IKKβ using tissue-specific knockouts, the effects of IKKβ in human PC cell lines using knockouts has not been adequately explored. We used CRISPR to knock out IKKβ (IKKβ KO) in MiaPaCa2 cells (*SI Appendix*, Fig. S1 *A* and *B*). The loss of IKKβ did not alter the levels of key molecules in the canonical NF-κB pathway (IKKα, IKKγ, IκBα, p65, and p105/p50) except in reduction in the levels of IκBα phosphorylation, the primary substrate for IKKβ (Fig. 1*A*) (25). Cell growth studies revealed that IKKβ was dispensable for growth in a cell line model and the presence or absence of IKKβ did not affect sensitivity to gemcitabine (Fig. 1*B* and

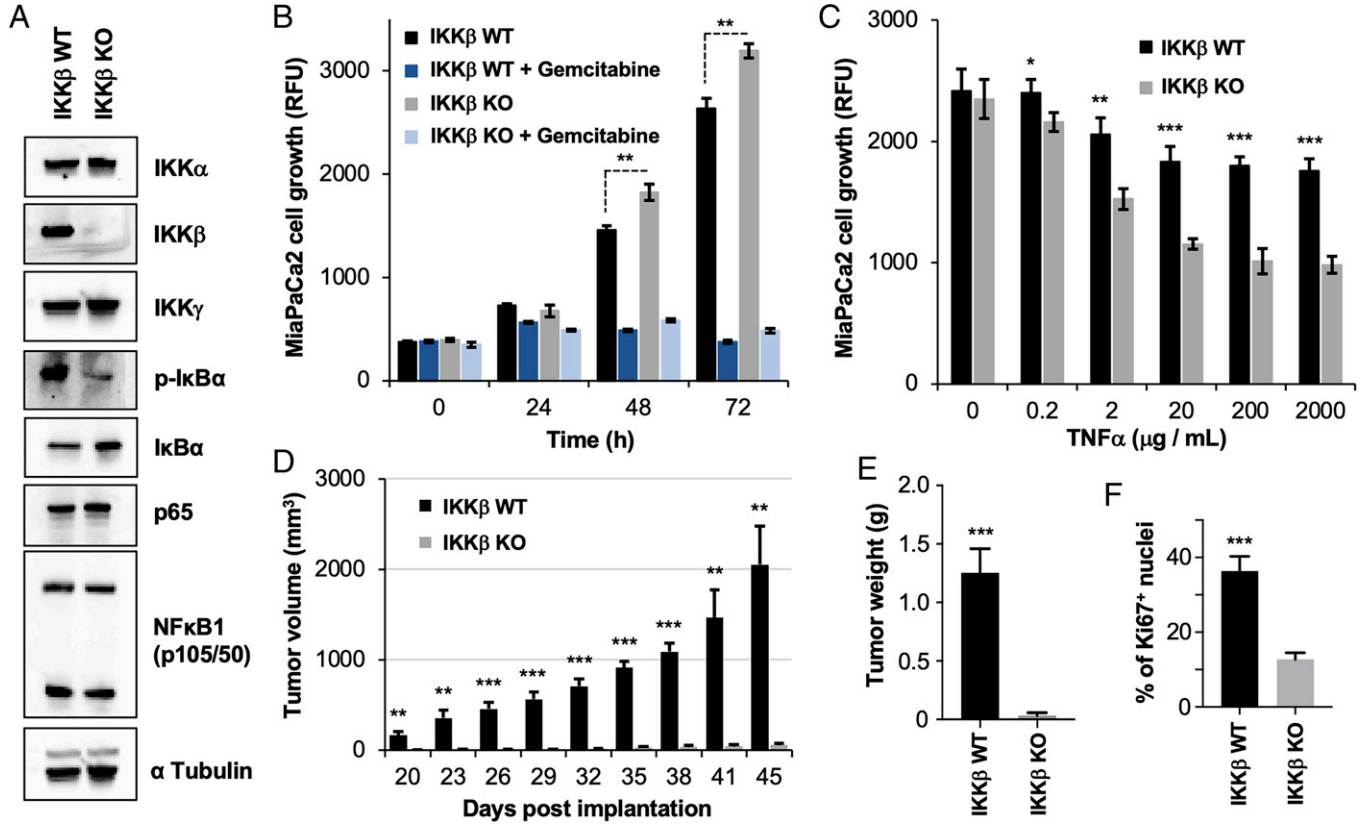

Fig. 1. IKKβ is dispensable for cell growth in two-dimensional models but is critical for pancreatic tumor growth. (*A*) Expression of canonical NF-κB pathway proteins in MiaPaCa2 IKKβ WT and IKKβ KO cells. Cell lysates were subjected to Western blotting and probed using the indicated antibodies. (*B*) A time-course study of growth of MiaPaCa2 IKKβ WT and IKKβ KO cells (4×10^3) in the presence and absence of 100 nM gemcitabine ($n = 3$). (*C*) Effect of TNF-α on the growth of MiaPaCa2 IKKβ WT and IKKβ KO cells (4×10^3) following 24-h incubation ($n = 3$). (*D*) MiaPaCa2 cells (2.5×10^6 cells) were subcutaneously implanted in athymic nude mice ($n = 5$). Tumor volumes were measured every 72 h. (*E*) Tumor weights measured at the end of the study. (*F*) K_i67 levels assessed by IHC at the end of the study. Data represented as average ± SEM; *P* value determined by two-tailed hypothesis, Student's *t* test. $^*P < 0.05$, $^{**}P < 0.005$, $^{***}P < 0.0005$.

SI Appendix, Fig. S1*C*). Mouse embryonic fibroblasts (MEFs) that lack IKKβ were sensitive to TNF-α–induced apoptosis, because the NF-κB pathway regulates the expression of antiapoptotic proteins (26). Consistent with this observation, IKKβ KO MEF and IKKβ KO MiaPaCa2 cells exhibited modest sensitivity to TNF-α–induced growth inhibition when compared to IKKβ WT cells (Fig. 1*C* and *SI Appendix*, Fig. S1*D*). No such effect was observed when the isogenic cell lines were subjected to insulin or epidermal growth factor (EGF) (*SI Appendix*, Fig. S1 *E–G*). The viability of IKKβ KO MEFs and the embryonic lethality of the corresponding mice prompted us to assess the effects of IKKβ on PC tumor growth. In a subcutaneous tumor model, we found a dramatic reduction in the size of tumors (Fig. 1 *D* and *E*) formed by IKKβ KO PC cells along with reduced proliferation and angiogenesis markers (Fig. 1*F* and *SI Appendix*, Fig. S1 *H* and *J*). Moreover, we observed reduced TNF-α levels in the IKKβ KO tumors (*SI Appendix*, Fig. S1*I*), indicating a feed-forward loop resulting in ca-IKKβ.

ca-IKKβ in PC. To determine the kinetics of TNF-α–induced activation and deactivation of IKKβ, we subjected immortalized human pancreatic Nestin-expressing (HPNE) cells and two PC cell lines (S2013 with $Kras^{G12D}$ and MiaPaCa2 with $Kras^{G12C}$) to TNF-α stimulation and monitored changes in p-IKKβ levels over time (Fig. 2 *A–C*). We observed rapid activation of IKKβ in all three cell lines (10 min after TNF-α treatment). The activation in HPNE cells was transient as reflected by the return of IKKβ to its resting state in ∼2 h. However, elevated levels of p-IKKβ were observed at the 2-h time point in the PC cell lines, suggesting sustained activation. Moreover, a subpopulation of IKKβ is phosphorylated even in the absence of TNF-α in PC cell lines, suggesting constitutive activation (compare "0 time point" lanes in Fig. 2 *A–C*). To determine if p-IKKβ is found in patient-derived pancreatic tumors and liver metastasis, we conducted IHC studies with tissue from the University of Nebraska Medical Center Rapid Autopsy Program for Pancreas (*SI Appendix*, Fig. S2) (27). We observed higher p-IKKβ levels in the primary tumor and liver metastases compared to the tumor stroma, acinar, and ductal cells, indicating constitutive activation in the tumors and liver metastases (Fig. 2 *D* and *E*). We previously showed that our ATP noncompetitive IKKβ inhibitor (13-197) allowed transient activation of IKKβ but inhibited sustained IKKβ activation (22, 23). Consistent with that, herein we observed a dose-dependent decrease in the levels of p-IKKβ, indicating that 13-197 modulates the levels of ca-IKKβ (Fig. 2*F*). Together our results suggest that ca-IKKβ contributes to PC and returning it to its resting state is a viable therapeutic option.

Optimization of 13-197 Leads to NCE 39-100 with Improved Stability and Oral Bioavailability. Despite the anticancer effects exhibited by 13-197 in multiple cancer models, it suffers from poor metabolic stability and low oral bioavailability (22–24, 28). To address these concerns, we synthesized a focused library of 13-197 analogs (Fig. 3*A* and *SI Appendix*, Fig. S3) and screened them in a cell-based luciferase reporter assay to identify inhibitors of TNF-α–induced IKKβ-mediated NF-κB activity (Fig. 3*B*). We found that replacing the metabolically liable furan rings in 13-197 with a single *N*-methylpyrazole ring yielded analog 5 with improved activity. Moving the bromine atom from the para-position in analog 5 to the meta-position in analog 12 further improved the activity. Analog 12 exhibited comparable potency to BMS345541, a well-characterized allosteric IKKβ inhibitor (22, 29). On the other hand, moving the bromine atom to the ortho position in analog 13 reduced the activity and introducing a thiazole ring in analog 14 resulted in a complete loss of activity (30).

To determine if replacing the furan rings with *N*-methylpyrazole resulted in improved metabolic stability, we incubated 13-197 and analog 12 with human liver S9 fraction and monitored their stability using liquid chromatography-tandem mass spectrometry (Fig. 4*A*). The half-life ($t_{1/2}$) of analog 12 was four-fold better than 13-197 (Fig. 4*A*). Since the para-position of the phenyl ring in acetanilide moieties are susceptible to

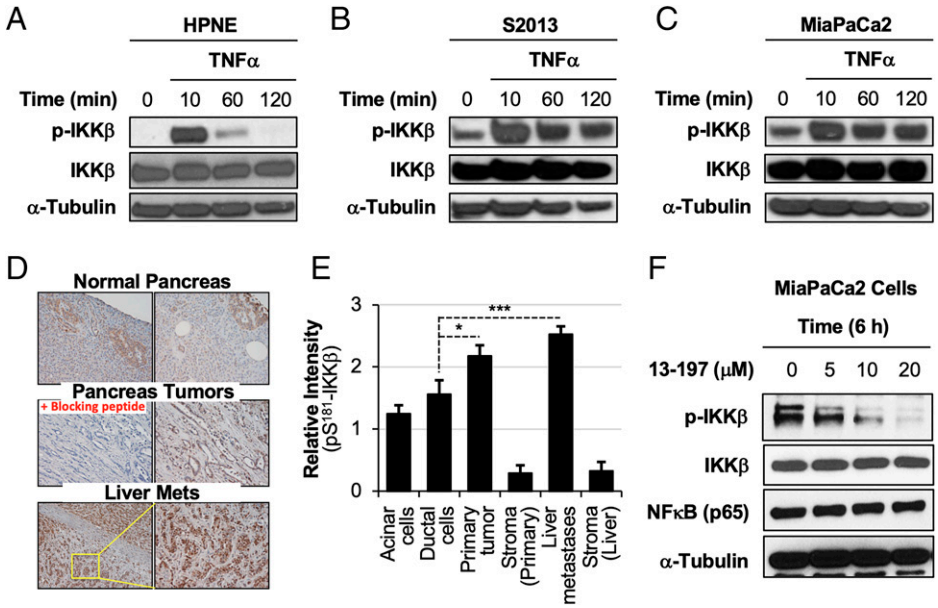

Fig. 2. Status of IKKβ phosphorylation in PC cell lines and in patient samples. (*A–C*) Time-course studies to assess the effect of TNF-α on the activation of IKKβ in HPNE ($Kras^{WT}$), S2013 ($Kras^{G12D}$), and MiaPaCa2 ($Kras^{G12C}$) cell lines. Cell lysates were subjected to Western blotting and probed using the indicated antibodies. (*D* and *E*) Tissue from normal pancreas ($n = 8$), pancreatic tumors and liver metastasis ($n = 40$) stained with phospho-(S^{181})-IKKβ antibody. Representative images are shown at 10x magnification (digital zoom). Data represented as average ± SEM; *P* value determined by one-tailed Student's *t* test $^*P < 0.05$, $^{***}P < 0.0005$. (*F*) A dose–response study to assess the effect of 13-197 on the activated IKKβ in MiaPaCa2 cells. Cell lysates were subjected to Western blotting and probed using the indicated antibodies.

A

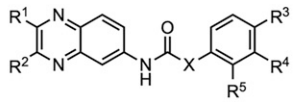

#	R^1	R^2	X	R^3	R^4	R^5
13-197	2-Furan	2-Furan	N	-Br	-H	-H
1	-H	2-Furan	N	-Br	-H	-H
2	2-Furan	-H	N	-Br	-H	-H
3	-H	3-Furan	N	-Br	-H	-H
4	3-Furan	-H	N	-Br	-H	-H
5	-H	3-(1-Me-1*H*-pyrazol-4-yl)	N	-Br	-H	-H
6	3-(1-Me-1*H*-pyrazol-4-yl)	-H	N	-Br	-H	-H
7	-H	3-(1-Me-1*H*-pyrazol-3-yl)	N	-Br	-H	-H
8	-H	3-(1*H*-pyrazol-4-yl)	N	-Br	-H	-H
9	-H	3-(1,3-diMe-1*H*-pyrazol-4-yl)	N	-Br	-H	-H
10	-H	3-(1-Me-1*H*-pyrazol-4-yl)	N	-H	-H	-H
11	-H	3-(1-Me-1*H*-pyrazol-4-yl)	C	-Br	-H	-H
12	-H	3-(1-Me-1*H*-pyrazol-4-yl)	N	-H	-Br	-H
13	-H	3-(1-Me-1*H*-pyrazol-4-yl)	N	-H	-H	-Br

B

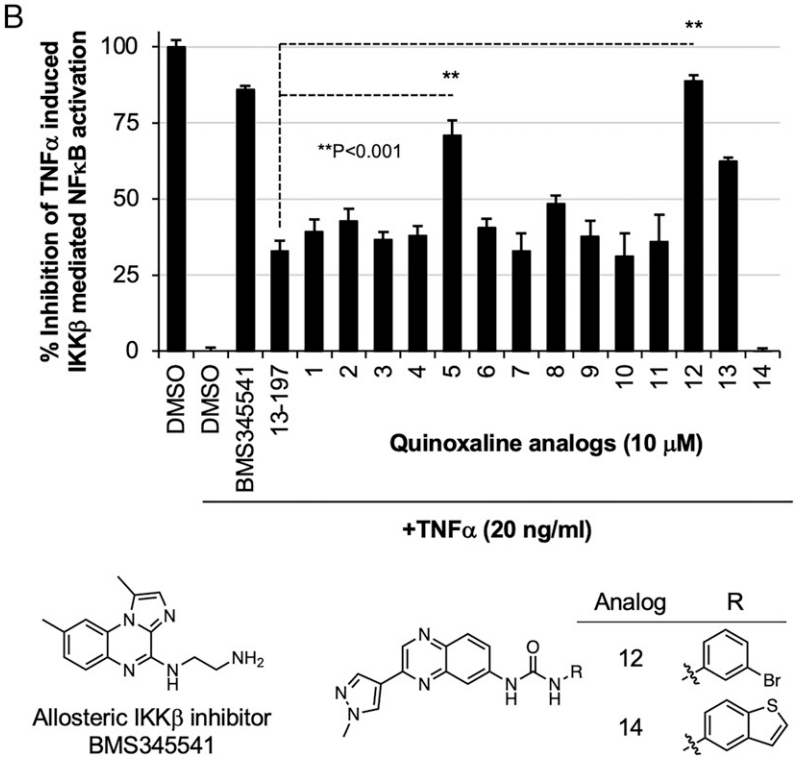

Fig. 3. SAR studies with quinoxaline analogs. (*A*) Structures of 13-197 and the quinoxaline analogs. (*B*) A dual luciferase assay-based screen to identify quinoxaline analogs that inhibit TNF-α–induced IKKβ-mediated NF-κB activation. Data represented are average ± SEM ($n = 4$), *P* value determined by two-tailed hypothesis Student's *t* test.

oxidation, we speculated that blocking it with a fluorine atom in analog 12 would further improve the stability. Indeed, the $t_{1/2}$ of 39-100 with an F-atom was approximately eight-fold better than 13-197 (Fig. 4*A*) and the major metabolites of 39-100 were demethylated, glucuronidated, and sulfated products (*SI Appendix*, Fig. S4 *A* and *B*). Importantly, BMS345541, analog 12, and 39-100 exhibited comparable potency in the TNF-α–induced IKKβ-mediated NF-κB activity assay (Fig. 4*B*). The systematic data-driven structural changes resulted in the improvement of oral bioavailability from ∼5% for 13-197 to ∼60% for 39-100 (Fig. 4*C* and *SI Appendix*, Fig. S4) (28). Together the iterative synthesis and screening led to the discovery of an NCE, 39-100, with an ∼8-fold and ∼12-fold improvement in stability and oral bioavailability, respectively.

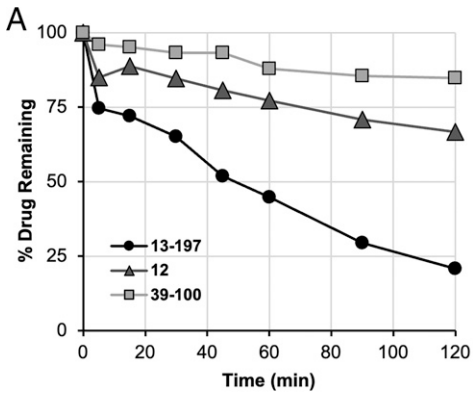

Quinoxaline analog	*in vitro* CL (μL / min / mg of protein)	$t_{1/2}$ (min)
13-197	12.2	57
12	2.9	242
39-100	1.6	436

B

Inhibitors	[a]IC_{50} ± SEM (μM)
BMS345541	5.6 ± 0.8
12	5.5 ± 0.6
39-100	4.7 ± 0.5

[a]TNFα induced IKKβ mediated NFκB activity

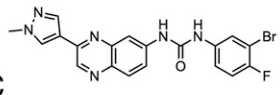

39-100
$C_{19}H_{14}BrFN_6O$
M. Wt. 440.0396

C

PK parameters	IV	Oral
	10 mg / kg	10 mg / kg
$T_{1/2}$ (h)	1.9 ± 0.4	2.0 ± 0.2
T_{max} (h)	-	3
Cmax (ng/mL)	4397 ± 430	694 ± 166
AUC_{last} (h*ng/mL)	9718 ± 1196	5948 ± 1898
AUC0-∞ (h*ng/mL)	9777 ± 1104	5950 ± 1898
MRT 0-∞ (h)	2.4 ± 0.3	5.3 ± 0.4
V_{ss} (L/kg)	2.4 ± 0.2	-
Bioavailability (%F)	-	60.9

Fig. 4. Discovery of 39-100 (IKAM-1), an orally bioavailable quinoxaline analog. (*A*) 13-197, 12, and IKAM-1 subjected to human liver S9 fraction. The table lists the clearance and half-life for the three analogs. (*B*) Evaluation of BMS345541, 12, and IKAM-1 in a luciferase reporter assay for the inhibition of TNF-α–induced IKKβ-mediated NF-κB activation in A549 cells (n = 3). (*C*) Oral and intravenous dose pharmacokinetic studies were performed in CD1 mice. The oral dose of IKAM-1 was 10 mg/kg, and the intravenous dose was 10 mg/kg. Data represented are average ± SD (n = 3).

39-100 (IKAM-1) Is a Selective MAP3K1 Inhibitor that Blocks Activation of IKKβ. To our surprise, unlike 13-197 (22), in in vitro assays 39-100 did not bind to or inhibit IKKβ (*SI Appendix*, Fig. S5 *A* and *B*). To identify the target, we subjected 39-100 and the inactive analog 14 to kinome profiling (KiNativ) in PANC1 cells (*SI Appendix*, Fig. S5*C*). Quantification of 337 kinase-associated peptides that correspond to 251 kinases revealed that 39-100 selectively binds to MAP3K1 and MAP3K12 and the inactive analog 14 did not. A follow-up dose–response study with 39-100 quantified 328 kinase-associated peptides that correspond to 254 kinases and showed selective dose-dependent ATP-competitive inhibition of MAP3K1 (Fig. 5*A* and *SI Appendix*, Table S1). Curve fitting the dose–response data resulted in an IC_{50} value of 4.2 ± 0.2 μM (*SI Appendix*, Fig. S5*D*). MAP3K1 is part of the STE branch of the kinome tree that has 47 kinases. The dose–response study quantified the levels of 22 of the 47 kinases in the STE branch. Selectivity of 39-100 for MAP3K1 is further demonstrated by a plot of the 10 closest kinases to MAP3K1 on the kinome tree and IKKβ (*SI Appendix*, Fig. S5*D*). Together, the data from our cellular dose–response kinome profiling reveals that 39-100 does not inhibit IKKβ but selectively inhibits MAP3K1 with micromolar potency in PANC1 cell lysates. IKKβ is a substrate of MAP3K1 (9) and consistently 39-100 reduced levels of p-IKKβ in a dose–response study (Fig. 5*B*), with an IC_{50} value of 2.3 ± 0.2 μM (*SI Appendix*, Fig. S5*E*). Since 39-100 is a selective MAP3K1 inhibitor that modulates IKKβ activation, we termed 39-100 as an IKKβ activation modulator (IKAM-1).

To validate MAP3K1 as the target of IKAM-1, we transiently transfected HeLa cells with MAP3K1-WT and MAP3K1-kinase dead (KD) mutants (31). Although modest, MAP3K1-WT–induced p-IKKβ was inhibited by IKAM-1 (Fig. 5*C* and *SI Appendix*, Fig. S5*F*). In addition, in MAP3K1-WT–transfected HeLa cells that stably express a luciferase reporter gene under the control of NF-κB response element, NF-κB activity was induced and no such increase was observed in the MAP3K1-KD–transfected cells (Fig. 5*D*). Moreover, TNF-α–induced MAP3K1-IKKβ–mediated NF-κB activation was inhibited by IKAM-1, while the control compound analog 14 did not (Fig. 5*D*). Although MAP3K12 was not inhibited by IKAM-1 in the dose–response study, to assess MAP3K12 contribution to the growth of PC cells, IKAM-1, analog 14, and DLK-In-1, a potent MAP3K12 inhibitor (K_i = 3 nM) (32), were subjected to growth inhibition studies in PC cell lines. IKAM-1 inhibits the growth of PC lines with low-micromolar potencies, while analog 14 or DLK-In-1 did not (Fig. 5*E* and *SI Appendix*, Fig. S5*G*). These data show that although 13-197 and IKAM-1 modulate p-IKKβ levels they exhibit different target profiles.

Characterization of IKAM-1 for TNF-α–Induced NF-κB Pathway-Selective Inhibition. Next, we assessed the ability of IKAM-1 to selectively inhibit TNF-α–induced MAP3K1-IKKβ–mediated NF-κB activity, using isogenic HeLa cell lines that stably express a luciferase reporter gene under the control of either NF-κB response element or p53 response element or AP1 response element. In dose–response studies, IKAM-1 selectively inhibited TNF-α–induced MAP3K1-IKKβ–mediated NF-κB activity but not Quinacrine-induced p53 activity or PMA-induced PKC-mediated AP1 activity (Fig. 6 *A*–*C*). Cyclic-pifithrin-α, a well-characterized small-molecule inhibitor of p53-dependent transactivation of p53-responsive genes, was used as positive control (33). Together, these results suggest that IKAM-1 binds to MAP3K1, blocks IKKβ activation to inhibit TNF-α–induced NF-κB activation.

Characterization of IKAM-1 in PC Cell Line and Animal Models. Next, we assessed the effects of analog 12 and IKAM-1 on NF-κB pathway proteins in a dose–response studies. Both analog 12 and IKAM-1 inhibited IκBα phosphorylation in a dose-dependent manner, suggesting inhibition of IKKβ activity. We previously showed that IKKβ inhibitors down-regulate Mcl-1 (23, 34); consistent with this observation, IKAM-1 and analog 12 showed robust reduction in Mcl-1 levels with no change in Bcl-xL. We also observed a dose-dependent increase in cleaved PARP, indicating the induction of apoptosis (*SI Appendix*, Fig. S6*A*). In a cell viability study with a panel of PC cell lines, analog 12 and IKAM-1 inhibited cell growth with low-micromolar potencies, which were comparable to an ATP-competitive IKKβ inhibitor (TPCA1) (35) and BMS345541 (Fig. 6*D* and

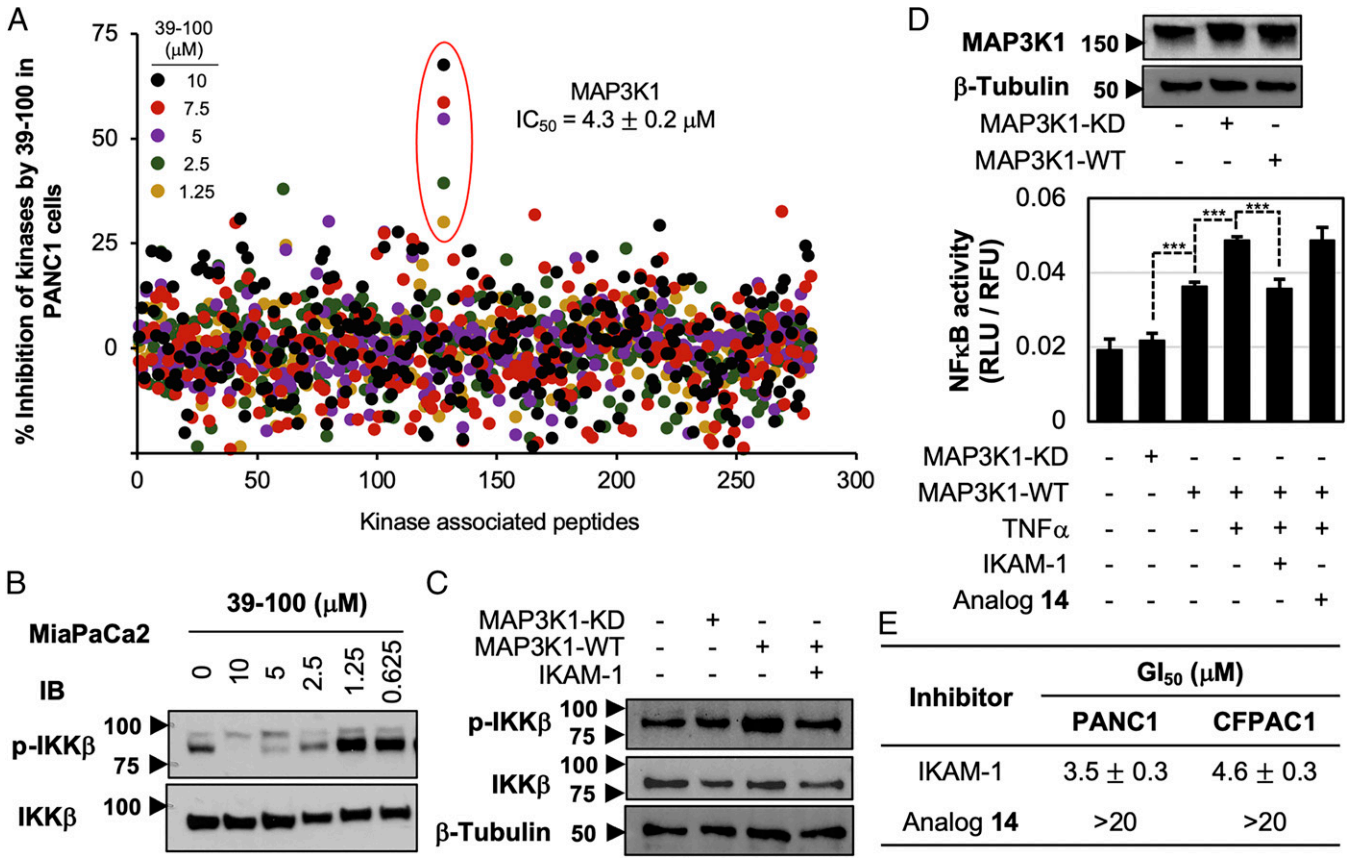

Inhibitor	GI_{50} (μM)	
	PANC1	CFPAC1
IKAM-1	3.5 ± 0.3	4.6 ± 0.3
Analog **14**	>20	>20

Fig. 5. Mechanism of action studies with IKAM-1. (*A*) Kinome profiling (KiNativ) dose–response study with IKAM-1 in PANC1 cells. Each spot represents a kinase inhibited by IKAM-1 at the indicated concentration (black: 10 μM; red: 7.5 μM; violet: 5 μM; green: 2.5 μM; and yellow: 1.25 μM). (*B*) MiaPaCa2 cells were treated with increasing concentrations of IKAM-1; the lysates were probed for p-IKKβ and IKKβ levels. (*C*) Western blot analyses with indicated antibodies of lysates from MAP3K1-KD (K1253M, V1467L) or MAP3K1 transfected HeLa cells in the presence and absence of IKAM-1. (*D*) MAP3K1-KD (K1253M, V1467L) or MAP3K1-WT were transiently transfected into HeLa cells that stably express a luciferase reporter gene under the control of an NF-κB response element. The MAP3K1 transfected cells were stimulated with TNF-α (20 ng/mL) for 6 h in the presence and absence of IKAM-1 or analog 14. The NF-κB activity was measured using luciferase reagent at the indicated conditions and normalized to cell viability. Data represented as average ± SD ($n = 3$). *P* value determined by two-tailed Student's *t* test, $^{***}P < 0.0005$. (*E*) Growth inhibition studies with IKAM-1, and analog 14 in PC cell lines (PANC1 and CFPAC1). Cell viability was determined using PrestoBlue following incubation of compounds for 72 h. Data represented are average ± SEM ($n = 3$).

SI Appendix, Fig. S6*B*). We compared the ability of IKAM-1 with TPCA1, BMS345541, and the Smac mimetic clinical candidate LCL161 to induce apoptosis. Results revealed that IKAM-1 induces caspase 3/7 mediated apoptosis and has comparable potencies with the IKKβ inhibitors and the Smac mimetic LCL161 in PC cell lines (Fig. 6*E*).

According to the human protein atlas database, the 5-y survival of PC patients with high MAP3K1 levels is 15%; however, this increases to 50% in PC patients with low MAP3K1 levels. This, along with the reports that show IKKβ plays a key role in KRAS mutation-associated PC, prompted us to assess the efficacy of IKAM-1 in orthotopic PC models. To test the efficacy of IKAM-1 in a syngeneic orthotopic model, C57BL/6 mice were orthotopically challenged with KrasG12D/Trp53R172H/Pdx1Cre (KPC) tumor cells (5×10^4) derived from a primary culture of spontaneously generated murine KPC tumor. Six days postchallenge, treatment cohorts began receiving daily oral administration of IKAM-1 (40 mg/kg) for 4 wk. IKAM-1 was formulated as previously described (28), and 100 μL of IKAM-1 solution was dosed daily by oral gavage. In parallel, we also treated mice with gemcitabine at 100 mg/kg every 4 d by intraperitoneal administration. Animal necropsies were generally unremarkable; with the exception of periodic gastric gas accumulation, IKAM-1–treated mice showed no apparent signs of toxicity. The final tumor volumes and weights from mice from the various groups are summarized in *SI Appendix*, Fig. S6 *C* and *D*. These results demonstrate that IKAM-1 does not exhibit any adverse effect in pancreatic tumor bearing mice with an intact immune system.

Next, we used an orthotopic xenograft model to assess the effects of IKAM-1 on pancreatic tumors derived from human cell lines to mimic late-stage pancreatic tumors in patients. Fourteen days postorthotopic implantation of PC cells (T3M4 with $Kras^{Q61H}$), mice were treated orally with either IKAM-1 (40 mg/kg) or vehicle. In IKAM-1–treated mice, we observed reduced tumor weight and tumor volume (Fig. 6 *F* and *G* and *SI Appendix*, Fig. S6*E*) when compared to vehicle-treated mice. Additionally, we observed reduced expression of p-IKKβ in the IKAM-1–treated tumors when compared to vehicle-treated tumors (Fig. 6*H* and *SI Appendix*, Fig. S6*F*), indicating in vivo target perturbation. We also observed reduced K_i67 and $CD31^+$ tumor cells in IKAM-1–treated tumors as compared to vehicle-treated tumors (*SI Appendix*, Fig. S6*G*). Consistent with reduced CD31 staining, we observed reduced metastasis to the peritoneum and liver, and no metastasis to lung and diaphragm in IKAM-1 as compared to vehicle-treated tumor-bearing animals (*SI Appendix*, Fig. S6*H*). Together, these results show that oral dosing of IKAM-1 reduced p-IKKβ levels in tumors, and reduced PC tumor growth and metastasis with no obvious toxicities (*SI Appendix*, Fig. S6*H*) in a human orthotopic xenograft model.

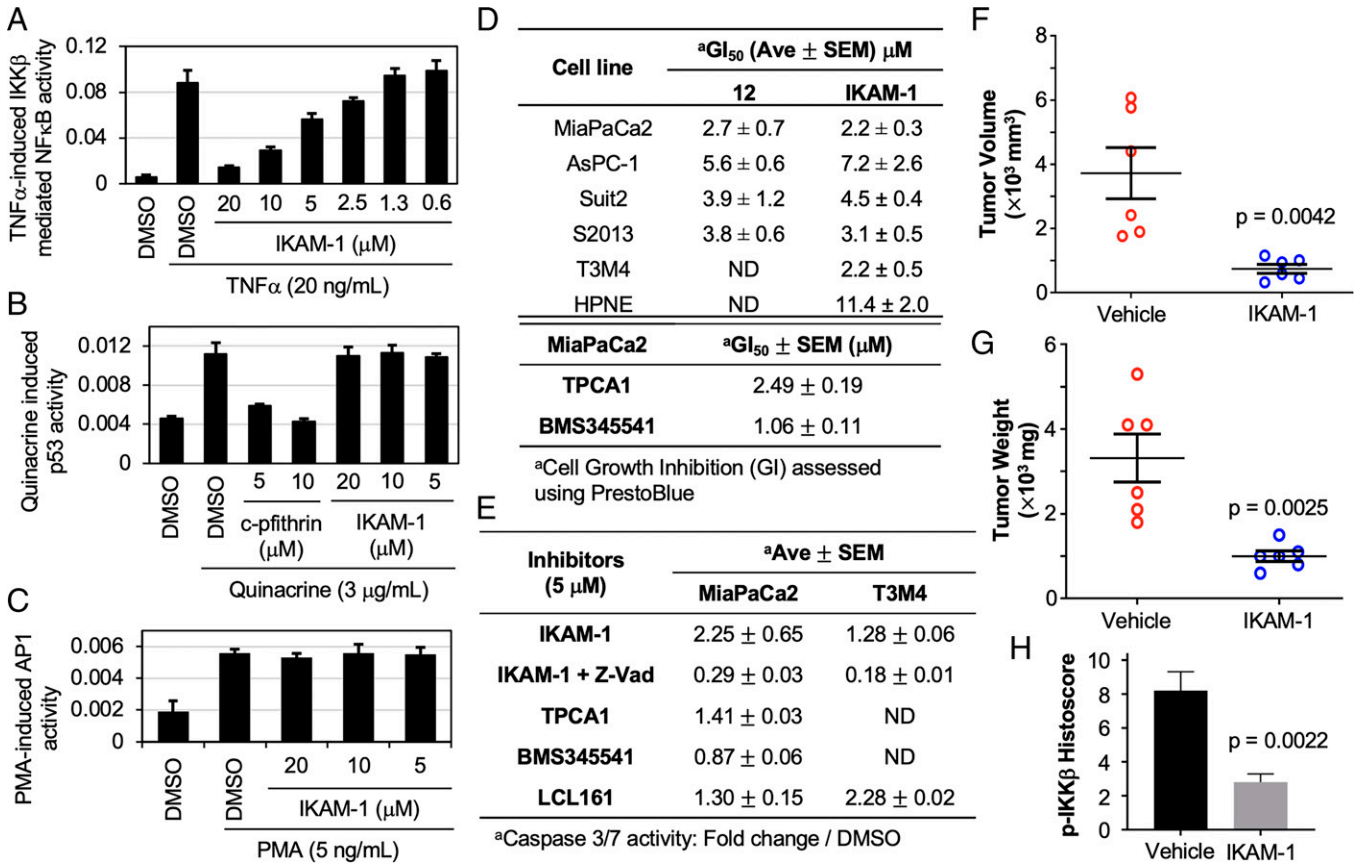

Fig. 6. Efficacy studies with IKAM-1 in PC models. (*A–C*) Evaluation of IKAM-1 for pathway specific inhibition in HeLa cell lines that stably express a luciferase reporter gene under the control of either NF-κB response element or p53 response element or AP1 response element ($n = 3$). (*D*) Growth inhibition studies with analog 12, IKAM-1, TPCA1, and BMS345541 in a panel of PC cell lines (MiaPaCa2, AsPC-1, Suit2, S2013, and T3M4). Cell viability was determined using PrestoBlue following incubation of compounds for 72 h ($n = 3$). (*E*) MiaPaCa2 and T3M4 cell lines were treated with IKAM-1, IKAM-1 + Z-Vad, TPCA1, BMS345541, or LCL161 for 24 h. Apoptosis assessed by measuring the induction of caspase 3/7 activity using the Caspase-Glo 3/7 system ($n = 3$). (*F* and *G*) IKAM-1 inhibits PC tumor growth. T3M4 cells (3×10^5 cells) were orthotopically implanted into the pancreas of athymic nude mice ($n = 6$). Tumors were treated with vehicle control and IKAM-1 (40 mg/kg, by mouth for 28 d). Tumor volume and weight were measured at the time of killing. (*H*) Average histoscore of p-IKKβ IHC in vehicle and IKAM-1–treated tumor-bearing animals ($n = 5$). Data represented as average ± SEM ($n = 5$), *P* value determined by unpaired Student's *t* test. ND, not determined.

Discussion

Our interest in IKKβ stemmed from elegant studies that reported pancreas-specific elimination of IKKβ resulted in stalling of Kras mutation-driven PC at the pancreatic intraepithelial neoplasia stage (5, 6). The reduced levels of p-IκBα observed in our IKKβ KO cells is consistent with previously reported elevated levels of nuclear RELA levels observed in majority of pancreatic ductal adenocarcinoma tumors (36). Unlike orthotopic implantation of AsPC-1 cells expressing the nonphosphorylated form of IκBα, which reduced metastasis but did not affect tumor growth (37), we found that IKKβ KO in MiaPaCa2 cells dramatically reduced tumor growth. The presence of elevated levels of nuclear RELA in most PC tumors but not in adjacent normal tissue indicates constitutive activation of IKKβ. Activated IKKβ protects cancer cells by regulating the levels of antiapoptotic proteins and in the presence of oncogenic insults drives tumor growth (3, 4). Consistent with the above, in patient-derived PC tissue we observed elevated levels of activated IKKβ in PC tumors and liver metastasis when compared to adjacent ductal cells or the stroma. Moreover, the presence of a subpopulation of ca-IKKβ in PC cells and, unlike in normal cells, the inability of PC cells to de-activate cytokine-induced activation of IKKβ implicates activated IKKβ as a viable target for PC therapy.

The development of ATP-competitive IKKβ inhibitors was stalled following unanticipated toxicities (7, 13). Imidazo[1,2-*a*] quinoxaline analog BMS345541, was the first allosteric IKKβ inhibitor that was reported and was shown to inhibit melanoma tumor growth in subcutaneous models (29, 38). Through iterative synthesis and screening we identified a quinoxaline urea analog 13-197 that inhibited PC tumor growth and metastasis (23, 34). More recently, we showed while BMS345541 does inhibit IKKβ in an ATP-competitive manner, 13-197 was an ATP noncompetitive IKKβ inhibitor (22). Here we show that 13-197 reduced p-IKKβ levels providing the molecular basis for the previously reported antitumor effects (23, 24).

A >30% rat oral bioavailability (F) is a go/no-go criteria for pretherapeutic lead compounds. This can be achieved for compounds such as 13-197 ($\%F^{rat} = 16$) through systematic structure-activity relationship (SAR) studies to engineer out functionality that are a metabolic liability (30, 39). We used 13-197 and the allosteric IKKβ inhibitor BMS345541 as control compounds to bookend the activity range for the TNF-α–induced IKKβ-mediated NF-κB activity assay (23, 29). The SAR study identified key functional groups required for activity and analog 12 exhibited comparable potency to the allosteric IKKβ inhibitor BMS345541, while analog 14 exhibited no inhibitory activity. Metabolic stability studies with liver microsomes showed that

replacing the furan rings in 13-197 with a hydrogen atom and 2-methylpyrazole in analog 12 resulted in an approximately four-fold improvement in the stability. It is known that the paraposition on acetanilide is susceptible to oxidation in the liver followed by elimination through either sulfation or glucuronidation (40). Therefore, a strategically placed F atom at the paraposition in IKAM-1 resulted in approximately eightfold improvement in the half-life when compared to 13-197. Metabolic profiling of IKAM-1 suggests that replacing the methyl group with a $-CF_3$ or a $-C_2H_5$ would further improve the stability of the compound. The addition of the F atom in IKAM-1 did not compromise its ability to inhibit TNF-α–induced IKKβ-mediated NF-κB activity and was more potent than 13-197.

Unexpectedly, unlike 13-197, IKAM-1 was inactive in in vitro IKKβ binding and enzymatic assays, however like 13-197 it was able to reduce p-IKKβ levels. Targeting upstream signaling components that result in the phosphorylation of IKKβ is an alternate approach to reduce p-IKKβ levels. An excellent example is the Bruton tyrosine kinase, which is upstream of IKKβ, and the Bruton tyrosine kinase inhibitor Ibrutinib is approved for the treatment of MCL. Sensitivity to Ibrutinib correlates with reduction in IκBα phosphorylation levels in MCL cell lines (41). Several upstream kinases, such as MAP3K1, PKC, TBK1, and TAK1, that were reported to activate IKKβ (10, 42, 43), and a chemoproteomic kinome profiling in PANC1 cells, identified MAP3K1 as the IKAM-1 target (44, 45). A follow-up dose–response study that assessed the ability of IKAM-1 to inhibit >250 kinases showed that IKAM-1 is a low-micromolar selective ATP-competitive MAP3K1 inhibitor.

MAP3K1 is a 196-kDa protein with a C-terminal kinase domain and an N-terminal regulatory domain with no known inhibitors. MAP3K1 is known to regulate AP1 and NF-κB transcription and a point mutant I1394A in the kinase domain of MAP3K1 minimally inhibited AP1 activity but completely abolished NF-κB activity (46). This is consistent with our observation that shows cellular selectivity of IKAM-1 for TNF-α–induced IKKβ-mediated NF-κB activity over the PMA-induced PKC-activated AP1 activity. Studies previously showed that MAP3K1 activates IKK resulting in the phosphorylation of the IKKβ substrate IκBα (9, 47). Expression of dominant-negative (DN) MAP3K1 in PC cell lines, an amnion-derived immortalized cell line (FL), and hepatocellular carcinoma cell line (Huh7) showed that DN-MAP3K1 expression resulted in reduction of the number of colonies only in PC cell lines but not in FL or Huh7 (48). Consistent with the above, IKAM-1 inhibited growth of PC cell lines with low-micromolar potency, while analog 14 did not, suggesting that IKAM-1 perturbs kinase activity of MAP3K1 to inhibit growth of PC cells. In addition to the IKKβ-mediated NF-κB pathway, MAP3K1 also promotes signaling through ERK, JNK, and p38 in response to different cellular cues. This is apparent in the differential growth effects observed in MiaPaCa2 cells in the absence of IKKβ vs. inhibition of MAP3K1 by IKAM-1.

There are a limited number of studies that explored perturbing IKKβ function in orthotopic pancreatic tumor models that mimics the human condition. The efficacy of orally administered IKAM-1 in syngeneic and xenograft PC orthotopic models was comparable to those reported with other modulators of IKKβ, which include NEMO binding peptide (intraperitoneally) in an HPNE/$Kras^{G12V}$/P16sh xenograft model and IKKβ inhibitors PS-1145 (intraperitoneally) in a PANC1 xenograft model (17, 49). Together these studies suggest that blocking MAP3K1-IKKβ–mediated activation of the NF-κB pathway could be explored as a therapeutic modality for PC.

In conclusion, we report the discovery of a small-molecule pair of IKAM-1/analog 14 that may be used to dissect the MAP3K1-IKKβ signaling axis in PC. Our findings suggests that MAP3K1-mediated IKKβ activation contributes to KRAS mutation-associated PC growth and IKAM-1 is a viable pre-therapeutic lead. Activation of parallel pathways is suggested as a major reason for the disappointing performance-targeted agents. In an elegant study, Xue et al. (50) recently showed that MAP3K1-mediated JNK-JUN activation contributes to MEK inhibitor resistance and predicted that small-molecule inhibitors of MAP3K1 will be synergistic with MEK inhibitors. Thus, the availability of IKAM-1 also facilitates future combination studies with not only clinically used MEK/ERK inhibitors but also compounds that target the NF-κB pathway proteins downstream of the IKK complex.

Materials and Methods

The complete experimental methods and materials used are included in *SI Appendix*. Details relate to all the materials used, including chemicals, antibodies, plasmids, cell lines, and animals. All animal experiments conducted were approved by the University of Nebraska Medical Center Institutional Animal Care and Use Committee. Experimental details include CRISPR-Cas9–mediated IKKβ KO cell line generation, synthesis protocols used to generate the analogs, and characterization of the intermediates and final products, cell viability assays, luciferase reporter assay, metabolic stability studies, DNA transfection, Western blotting, caspase 3/7 assay, pharmacokinetic studies, IHC, and orthotopic PC models.

Data Availability. All study data are included in the main text and *SI Appendix*.

ACKNOWLEDGMENTS. We thank T. Caffrey, R. M. Quadros, Dr. C. B. Gurumurthy, and Dr. Ben Swanson for technical assistance. This work was supported in part by NIH Grants CA182820, CA197999, CA251151, CA208108, CA210240, CA211462, CA127297, and CA036727. H.M.K. and S. Kour were supported by a University of Nebraska Medical Center fellowship. L.B. was supported by NIH Grant CA009476.

Author affiliations: [a]Eppley Institute for Cancer Research, University of Nebraska Medical Center, Omaha, NE 68198; [b]Department of Pharmaceutical Sciences, University of Nebraska Medical Center, Omaha, NE 68198; [c]Gene Editing Institute, Christiana Care, Newark, DE 19713; [d]Department of Genetics Cell Biology and Anatomy, University of Nebraska Medical Center, Omaha, NE 68198; and [e]Fred & Pamela Buffett Cancer Center, University of Nebraska Medical Center, Omaha, NE 68198

1. F. Mercurio *et al.*, IKK-1 and IKK-2: Cytokine-activated IkappaB kinases essential for NF-kappaB activation. *Science* **278**, 860–866 (1997).
2. D. F. Lee *et al.*, IKK beta suppression of TSC1 links inflammation and tumor angiogenesis via the mTOR pathway. *Cell* **130**, 440–455 (2007).
3. M. Naramura, A. Natarajan, Mouse pancreatic tumor model independent of tumor suppressor gene inactivation. *Pancreas* **47**, e27–e29 (2018).
4. H. Shaked *et al.*, Chronic epithelial NF-κB activation accelerates APC loss and intestinal tumor initiation through iNOS up-regulation. *Proc. Natl. Acad. Sci. U.S.A.* **109**, 14007–14012 (2012).
5. J. Ling *et al.*, KrasG12D-induced IKK2/β/NF-κB activation by IL-1α and p62 feedforward loops is required for development of pancreatic ductal adenocarcinoma. *Cancer Cell* **21**, 105–120 (2012).
6. E. Maniati *et al.*, Crosstalk between the canonical NF-κB and Notch signaling pathways inhibits Pparγ expression and promotes pancreatic cancer progression in mice. *J. Clin. Invest.* **121**, 4685–4699 (2011).
7. Y. Xia *et al.*, Reduced cell proliferation by IKK2 depletion in a mouse lung-cancer model. *Nat. Cell Biol.* **14**, 257–265 (2012).
8. J. Yang *et al.*, Conditional ablation of Ikkb inhibits melanoma tumor development in mice. *J. Clin. Invest.* **120**, 2563–2574 (2010).
9. F. S. Lee, J. Hagler, Z. J. Chen, T. Maniatis, Activation of the IkappaB alpha kinase complex by MEKK1, a kinase of the JNK pathway. *Cell* **88**, 213–222 (1997).
10. J. Zhang, K. Clark, T. Lawrence, M. W. Peggie, P. Cohen, An unexpected twist to the activation of IKKβ: TAK1 primes IKKβ for activation by autophosphorylation. *Biochem. J.* **461**, 531–537 (2014).

11. S. Tegethoff, J. Behlke, C. Scheidereit, Tetrameric oligomerization of IkappaB kinase gamma (IKKgamma) is obligatory for IKK complex activity and NF-kappaB activation. *Mol. Cell. Biol.* **23**, 2029–2041 (2003).
12. K. Nagashima *et al.*, Rapid TNFR1-dependent lymphocyte depletion in vivo with a selective chemical inhibitor of IKKbeta. *Blood* **107**, 4266–4273 (2006).
13. F. R. Greten *et al.*, NF-kappaB is a negative regulator of IL-1beta secretion as revealed by genetic and pharmacological inhibition of IKKbeta. *Cell* **130**, 918–931 (2007).
14. J. A. DiDonato, F. Mercurio, M. Karin, NF-κB and the link between inflammation and cancer. *Immunol. Rev.* **246**, 379–400 (2012).
15. C. Gamble *et al.*, Inhibitory kappa B Kinases as targets for pharmacological regulation. *Br. J. Pharmacol.* **165**, 802–819 (2012).
16. J. A. Prescott, S. J. Cook, Targeting IKKβ in cancer: Challenges and opportunities for the therapeutic utilisation of IKKβ inhibitors. *Cells* **7**, 115 (2018).
17. Z. Zhuang *et al.*, NEMO peptide inhibits the growth of pancreatic ductal adenocarcinoma by blocking NF-κB activation. *Cancer Lett.* **411**, 44–56 (2017).
18. J. Totzke *et al.*, Takinib, a selective TAK1 inhibitor, broadens the therapeutic efficacy of TNF-α inhibition for cancer and autoimmune disease. *Cell Chem. Biol.* **24**, 1029–1039.e7 (2017).
19. G. Xu *et al.*, Crystal structure of inhibitor of κB kinase β. *Nature* **472**, 325–330 (2011).
20. S. Polley *et al.*, A structural basis for IκB kinase 2 activation via oligomerization-dependent trans auto-phosphorylation. *PLoS Biol.* **11**, e1001581 (2013).
21. S. Liu *et al.*, Crystal structure of a human IκB kinase β asymmetric dimer. *J. Biol. Chem.* **288**, 22758–22767 (2013).
22. J. V. Napoleon *et al.*, Small molecule binding to inhibitor of nuclear factor kappa-B kinase subunit beta in an ATP non-competitive manner. *Chem. Commun. (Camb.)* **57**, 4678–4681 (2021).
23. P. Radhakrishnan *et al.*, Targeting the NF-κB and mTOR pathways with a quinoxaline urea analog that inhibits IKKβ for pancreas cancer therapy. *Clin. Cancer Res.* **19**, 2025–2035 (2013).
24. N. K. Chaturvedi *et al.*, Novel treatment for mantle cell lymphoma including therapy-resistant tumor by NF-κB and mTOR dual-targeting approach. *Mol. Cancer Ther.* **12**, 2006–2017 (2013).
25. E. Zandi, Y. Chen, M. Karin, Direct phosphorylation of IkappaB by IKKalpha and IKKbeta: Discrimination between free and NF-kappaB-bound substrate. *Science* **281**, 1360–1363 (1998).
26. Q. Li, D. Van Antwerp, F. Mercurio, K. F. Lee, I. M. Verma, Severe liver degeneration in mice lacking the IkappaB kinase 2 gene. *Science* **284**, 321–325 (1999).
27. H. C. Law *et al.*, The proteomic landscape of pancreatic ductal adenocarcinoma liver metastases identifies molecular subtypes and associations with clinical response. *Clin. Cancer Res.* **26**, 1065–1076 (2020).
28. N. Gautam, S. P. Bathena, Q. Chen, A. Natarajan, Y. Alnouti, Pharmacokinetics, protein binding and metabolism of a quinoxaline urea analog as an NF-κB inhibitor in mice and rats by LC-MS/MS. *Biomed. Chromatogr.* **27**, 900–909 (2013).
29. J. Yang, K. I. Amiri, J. R. Burke, J. A. Schmid, A. Richmond, BMS-345541 targets inhibitor of kappaB kinase and induces apoptosis in melanoma: Involvement of nuclear factor kappaB and mitochondria pathways. *Clin. Cancer Res.* **12**, 950–960 (2006).
30. S. Sagar *et al.*, Structure activity relationship (SAR) study identifies a quinoxaline urea analog that modulates IKKβ phosphorylation for pancreatic cancer therapy. *Eur. J. Med. Chem.* **222**, 113579 (2021).
31. C. Widmann, P. Gerwins, N. L. Johnson, M. B. Jarpe, G. L. Johnson, MEK kinase 1, a substrate for DEVD-directed caspases, is involved in genotoxin-induced apoptosis. *Mol. Cell. Biol.* **18**, 2416–2429 (1998).
32. S. Patel *et al.*, Selective inhibitors of dual leucine zipper kinase (DLK, MAP3K12) with activity in a model of Alzheimer's disease. *J. Med. Chem.* **60**, 8083–8102 (2017).
33. N. Pietrancosta *et al.*, Novel cyclized Pifithrin-alpha p53 inactivators: Synthesis and biological studies. *Bioorg. Med. Chem. Lett.* **15**, 1561–1564 (2005).
34. R. Rajule, V. C. Bryant, H. Lopez, X. Luo, A. Natarajan, Perturbing pro-survival proteins using quinoxaline derivatives: A structure-activity relationship study. *Bioorg. Med. Chem.* **20**, 2227–2234 (2012).
35. P. L. Podolin *et al.*, Attenuation of murine collagen-induced arthritis by a novel, potent, selective small molecule inhibitor of IkappaB Kinase 2, TPCA-1 (2-[(aminocarbonyl)amino]-5-(4-fluorophenyl)-3-thiophenecarboxamide), occurs via reduction of proinflammatory cytokines and antigen-induced T cell Proliferation. *J. Pharmacol. Exp. Ther.* **312**, 373–381 (2005).
36. W. Wang *et al.*, The nuclear factor-kappa B RelA transcription factor is constitutively activated in human pancreatic adenocarcinoma cells. *Clin. Cancer Res.* **5**, 119–127 (1999).
37. S. Fujioka *et al.*, Function of nuclear factor kappaB in pancreatic cancer metastasis. *Clin. Cancer Res.* **9**, 346–354 (2003).
38. J. R. Burke *et al.*, BMS-345541 is a highly selective inhibitor of I kappa B kinase that binds at an allosteric site of the enzyme and blocks NF-kappa B-dependent transcription in mice. *J. Biol. Chem.* **278**, 1450–1456 (2003).
39. V. H. Thomas *et al.*, The road map to oral bioavailability: An industrial perspective. *Expert Opin. Drug Metab. Toxicol.* **2**, 591–608 (2006).
40. J. L. Cunningham, M. J. Leyland, I. W. Delamore, D. A. Evans, Acetanilide oxidation in phenylbutazone-associated hypoplastic anaemia. *BMJ* **3**, 313–317 (1974).
41. R. Rahal *et al.*, Pharmacological and genomic profiling identifies NF-κB-targeted treatment strategies for mantle cell lymphoma. *Nat. Med.* **20**, 87–92 (2014).
42. H. Nakano *et al.*, Differential regulation of IkappaB kinase alpha and beta by two upstream kinases, NF-kappaB-inducing kinase and mitogen-activated protein kinase/ERK kinase kinase-1. *Proc. Natl. Acad. Sci. U.S.A.* **95**, 3537–3542 (1998).
43. T. Weng, C. G. Koh, POPX2 phosphatase regulates apoptosis through the TAK1-IKK-NF-κB pathway. *Cell Death Dis.* **8**, e3051 (2017).
44. M. P. Patricelli *et al.*, In situ kinase profiling reveals functionally relevant properties of native kinases. *Chem. Biol.* **18**, 699–710 (2011).
45. C. E. Franks, K. L. Hsu, Activity-based kinome profiling using chemical proteomics and ATP acyl phosphates. *Curr. Protoc. Chem. Biol.* **11**, e72 (2019).
46. Z. Tu, F. S. Lee, Subdomain VIII is a specificity-determining region in MEKK1. *J. Biol. Chem.* **278**, 48498–48505 (2003).
47. M. Hirano *et al.*, MEK kinase is involved in tumor necrosis factor alpha-induced NF-kappaB activation and degradation of IkappaB-alpha. *J. Biol. Chem.* **271**, 13234–13238 (1996).
48. T. Hirano *et al.*, Dominant negative MEKK1 inhibits survival of pancreatic cancer cells. *Oncogene* **21**, 5923–5928 (2002).
49. Y. Zhang *et al.*, IkappaBalpha kinase inhibitor IKI-1 conferred tumor necrosis factor alpha sensitivity to pancreatic cancer cells and a xenograft tumor model. *Cancer Res.* **68**, 9519–9524 (2008).
50. Z. Xue *et al.*, MAP3K1 and MAP2K4 mutations are associated with sensitivity to MEK inhibitors in multiple cancer models. *Cell Res.* **28**, 719–729 (2018).